THE ASTROPHYSICAL JOURNAL, 352:1–14, 1990 March 20

TOPOLOGY OF MICROWAVE BACKGROUND FLUCTUATIONS: THEORY

J. RICHARD GOTT III AND CHANGBOM PARK
Department of Astrophysical Sciences, Princeton University

ROMAN JUSZKIEWICZ
Institute for Advanced Study, Princeton; and Copernicus Center, Warsaw, Poland

WILLIAM E. BIES AND DAVID P. BENNETT
Physics Department and Department of Astrophysical Sciences, Princeton University

FRANÇOIS R. BOUCHET
Institut d'Astrophysique de Paris, Paris, France; and Centre de Physique Theorique Ecole Polytechnique

AND

ALBERT STEBBINS
Canadian Institute for Theoretical Astrophysics, Toronto, Canada
Received 1989 July 3; accepted 1989 September 19

ABSTRACT

Topological measures are used to characterize the microwave background temperature fluctuations produced by "standard" scenarios (Gaussian) and by cosmic strings (non-Gaussian). Three topological quantities: total area of the excursion regions, total length, and total curvature (genus) of the isotemperature contours, are studied for simulated Gaussian microwave background anisotropy maps and then compared with those of the non-Gaussian anisotropy pattern produced by cosmic strings.

In general, the temperature gradient field shows the non-Gaussian behavior of the string map more distinctively than the temperature field for all topology measures. The total contour length and the genus are found to be more sensitive to the existence of a stringy pattern than the usual temperature histogram. Situations when instrumental noise is superposed on the map, are considered to find the critical signal-to-noise ratio for which strings can be detected. With current observational sensitivity (5 mK $Hz^{-1/2}$) and a 32 receiver array, 660 hr of mapping would demonstrate the non-Gaussian behavior due to cosmic strings if $G\mu > 6 \times 10^{-6}$. If such an observational program failed to detect any signals beyond instrumental noise, using our topological analysis we would be able to set limits of $G\mu < 4 \times 10^{-7}$ for strings and $\langle a_2^2 \rangle^{1/2} \leq 8 \times 10^{-7}$ for the Zel'dovich spectrum.

Subject heading: cosmic background radiation

I. INTRODUCTION

Microwave background radiation (hereafter MBR) has received much attention since its discovery 25 years ago (Penzias and Wilson 1965). Its spectrum is close to that of a blackbody with mean temperature $T = 2.74 \pm 0.016$ K (Wilkinson 1988), and it shows a dipole anisotropy with amplitude $\Delta T/T \approx 10^{-3}$ toward the direction $\alpha = 11^h.3 \pm 0^h.16$ and $\delta = -7°.5 \pm 2°.5$ (Smoot and Lubin 1979; Fixen, Cheng, and Wilkinson 1983; Lubin *et al.* 1985) which is attributed to the Earth's motion. Once the dipole term is subtracted, $\Delta T/T \leq 10^{-4}$ over all scales greater than 1′.

It is generally believed that intrinsic MBR anisotropies will be detected in the near future because the sensitivity of observation has reached the values predicted by realistic galaxy formation models. The *Cosmic Background Explorer* (*COBE*), scheduled to fly this year is expected to map the sky with sensitivity of $\Delta T/T \approx 3 \times 10^{-6}$ and angular resolution of 7°. The Soviet satellite *Relict 2*, planned for 1992 should reach the 10^{-6} level as well. At the same time, anisotropies at the 10^{-5} to 5×10^{-6} level seem inevitable. For example, the cold dark matter (CDM) model with Gaussian, adiabatic, scale-invariant initial fluctuations in a flat ($\Omega = 1$) universe with a baryon content $\Omega_B < 0.1$ and a Hubble constant of 50 km s^{-1} Mpc, predicts $(\Delta T/T)_{\rm rms} = 10^{-5}/b$ over a 7° scale (Bond 1988; Vittorio and Juszkiewicz 1987). Here $1.5 \leq b \leq 2.5$ is the so-called biasing parameter (Bardeen *et al.* 1986). Similar anisotropies on comparable angular scales ($\Delta T/T \sim 10^{-5}$ at several degrees) arise in the baryon-dominated universes with isocurvature fluctuations (Peebles 1987). This family of models was introduced when it became less clear that the CDM model could account for the large-scale structure observed in the peculiar velocity field and the spatial distribution of clusters. The common feature that these models share with CDM is the Gaussian nature of the initial density field. A non-Gaussian pattern is expected to arise in scenarios with massive cosmic strings which can be parameterized by their energy per unit length, μ. The preferred value is $G\mu \sim 10^{-6}$ (Brandenberger 1988). String networks normalized to this value are expected to generate $(\Delta T/T)_{\rm rms} \approx 2 \times 10^{-5}$ over scales in the range 7°–40° (Bouchet, Bennet and Stebbins 1988).

In order to investigate the geometrical nature of the MBR anisotropy we have to map a finite region of the sky. Statistical properties such as Gaussian behavior and the power spectrum of the temperature field may be determined by studying the excursion regions enclosed by isotemperature contours. Local geometrical information about the spatial structures is contained in three quantities: total area of excursion regions, total contour length, and curvature of the isotemperature contours. These are local and invariant quantities of the contours in the sense that they can be calculated even from a temperature map

with incomplete and patchy coverage and do not change under translation and rotation of the coordinate frame. If all excursion regions are compact, the Gauss-Bonnet theorem applies and the total curvature of the contours or the curvature integrated along all contours is proportional to the Euler-Poincare characteristic (EPC hereafter) of the excursion regions. At high threshold levels the excursion regons of a random temperature field will appear as isolated hot spots surrounded by the cold background and the total curvature will be positive. At low-temperature thresholds the contours surround cold spots and the total curvature is negative. Near the mean temperature the excursion regions and the cold regions are nearly symmetric, and the total curvature is close to zero. For a one-dimensional scan of the sky the relevant statistic is the number of upcrossings above the threshold which has been studied by Coles and Barrow (1987).

The study of curvature has been done for the smoothed galaxy density distribution in three-dimensional Euclidean space in order to find the nature of the initial density fluctuations and the subsequent evolution of the large-scale structures (Gott, Melott, and Dickinson 1986; Hamilton, Gott, and Weinberg 1986; Melott, Weinberg, and Gott 1988). Comparing the observed universe with many simulated ones, they found that over scales significantly larger than the galaxy correlation length the topology of isodensity surfaces of galaxy distribution is spongelike consistent with the random quantum noise scenario. When the scale is comparable to the correlation length, they found a small shift in the direction of a meatball topology which might be explained by biased CDM models (Gott *et al.* 1989).

The study of two-dimensional topology for astronomical random fields has just begun. Bond and Efstathiou (1987) and Vittorio and Juszkiewicz (1987) have studied peak statistics. Recently, Coles (1988) has proposed the integral geometric characteristic (hereafter IGC, see § II) as a sensitive discriminator between Gaussian and non-Gaussian MBR fields. Using Adler's results (1981), he gives formulae for the mean values of IGC for Gaussian and several non-Gaussian fields. Melott *et al.* (1989) have developed a similar statistic, the genus, and applied it to two-dimensional cross sections of simulated density fields of large-scale structure. It is the purpose of this paper to develop and apply this statistic to simulated MBR maps. We find the typical behavior of the topological measures for the standard Gaussian MBR map and their sensitivity to the existence or to the non-Gaussian behavior of the signal when instrumental noise is superposed on the ideal map. Particular emphasis is placed on the temperature gradient map because it is the direct output of a usual observation of MBR anisotropy (i.e., a beam subtraction experiment) and its geometry is very sensitive to cosmic strings.

In § II we define the genus as an integral of the curvature along contours on a two-dimensional Euclidean surface (i.e., a map over a small patch of the sky) and on the surface of a sphere (i.e., an all-sky map). In § III theoretical formulae of the topology measures (i.e., area of excursion regions, contour length, genus) for both Gaussian temperature and temperature gradient fields are presented for plane contours and for curves on a sphere. In § IV*a* those topological parameters are calculated from simulated Gaussian MBR maps: a $10^\circ \times 10^\circ$ map from the standard scenario, and all-sky maps with Zel'dovich and Poisson power spectra. In § IV*b* we test the sensitivity of the statistics to the existence of the string-pattern by using a χ^2 test which measures the deviation of the topological quantities from the mean values of the assumed Gaussian model. Finally, the statistics proposed for studying the MBR anisotropy and large-scale density fields are compared, and the application of our topological analysis to observed maps is discussed.

II. TOPOLOGICAL PARAMETERS

In this section we will define the genus of the excursion set for a random temperature field on a plane or on the curved surface of a sphere. The genus G can be loosely defined in two dimensions as

G = number of isolated high-temperature regions

− number of isolated low-temperature regions .

We will consider local properties like contour length and curvature which are invariant under translation and rotation of the coordinate frame. Then the genus can be defined as a measure of the total curvature of the contours.

First consider a differentiable curve C in a plane parameterized by $\boldsymbol{x} = \boldsymbol{x}(s)$ where s is the proper length. We orient the curve in such a way that it encloses the excursion domain counterclockwise. Let $\boldsymbol{t}(s) = (d\boldsymbol{x}/ds)/|d\boldsymbol{x}/ds|$ be the unit tangent vector at a point on the curve. The curvature $\kappa(s)$ is defined as

$$\kappa(s) = \pm \lim_{\Delta s \to 0} \frac{|\boldsymbol{t}(s + \Delta s) - \boldsymbol{t}(s)|}{\Delta s} = \pm \lim_{\Delta s \to 0} \frac{|\Delta \tau|}{\Delta s} = \frac{d\tau}{ds}, \quad (1)$$

where τ is the angle of the tangent vector $\boldsymbol{t}$ with a fixed direction. Notice that κ is an invariant of C in the sense that it is independent of coordinate translation, rotation, and of parameterization. The total curvature of C is defined as the integral

$$K = \int_C \kappa \, ds = \int_C d\tau . \quad (2)$$

Now we define the genus as the rotation index of the curve enclosing the excursion domain or the total curvature divided by 2π,

$$G = \frac{1}{2\pi} \int_C \kappa \, ds . \quad (3)$$

The theorem of turning tangents (Willmore 1982, p. 52) shows that the genus of a closed plane curve is ± 1 whose sign depends on its orientation.

If C is approximated by oriented line segments and we denote by $(\Delta\tau)_i$ the exterior angle at the ith corner, i.e., the angle between two vectors tangent to the two neighboring edges, the genus becomes

$$G = \frac{1}{2\pi} \sum_i (\Delta\tau)_i . \quad (4)$$

When we are considering contours defined by a threshold level of a random temperature field, a high level excursion will contribute $+1$ to the genus and a low-density hole in it will decrease the genus by 1. Therefore the genus can be considered as the total number of connected high-density regions minus the total number of holes in them. In practice, contours may cross the edge of the survey region, in which case the partial curves contribute noninteger rotation indices to the genus unless the boundary is periodic.

A statistic which has a very similar definition is the IGC Γ (Adler 1981). It is the number of high-density excursions e not intercepted by lower boundaries of survey intervals (i.e., $x = 0$

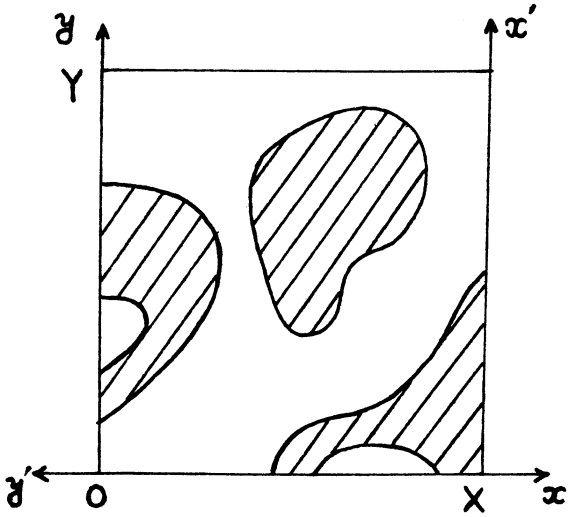

FIG. 1.—An illustration of the boundary effect on the value of the IGC

and $y = 0$ lines when the x and y intervals of the survey region is $[0, X]$, and $[0, Y]$) minus the number of holes in them h not intercepted by the upper boundaries (i.e., $x = X$, $y = Y$ lines). It is essentially the generalization of the level up-crossing statistic in one-dimension to higher dimensions. In Figure 1, for example, $e = 1$ and $h = 2$ which result in $\Gamma = e - h = -1$. If we rotate the coordinate axes by 90° (primed coordinate system), however, $e = 2$, $h = 1$ and $\Gamma = 1$. Therefore the IGC depends on the coordinate system while the genus does not. This difference becomes negligible as the survey region contains many structures not intercepted by the boundaries. If the excursion domains do not cross the boundaries or if the boundaries are periodic, both G and Γ become the EPC χ of the excursion regions, given by the Gauss-Bonnet theorem (Adler 1981; Willmore 1982):

$$\chi = \frac{1}{2\pi}\int \kappa\, ds\,. \tag{5}$$

Now consider a curve on a unit sphere S with coordinates (θ, ϕ). Since a "straight line" on a sphere is the geodesic line, we are interested in the geodesic curvature κ_g. Suppose we have an excursion domain A on S whose boundary C is parameterized by s. If A does not contain the poles where our coordinates fail to parameterize S, the geodesic curvature κ_g of C which is the measure of geodesic deviation of the contour line, is given by (Willmore 1982, p. 56)

$$\kappa_g\, ds = d\tau + \cos(\theta) d\phi\,, \tag{6}$$

where $\tau(s)$ is the oriented angle of the tangent vector with respect to the unit vector θ.

If C consists of piecewise differential curves L_i, the total rotation index or the genus is

$$\begin{aligned} G_s &= \frac{1}{2\pi}\sum_i \left[\int_{L_i} d\tau + (\Delta\tau)_i\right] \\ &= \frac{1}{2\pi}\sum_i \left[\int_{L_i} \kappa_g\, ds + (\Delta\tau)_i - \int_{L_i} \cos(\theta) d\phi\right] \\ &= \frac{1}{2\pi}\left[\int_C \kappa_g\, ds + \sum_i (\Delta\tau)_i - \int_C \cos(\theta) d\phi\right], \end{aligned} \tag{7}$$

where $(\Delta\tau)_i$ is the angle between two tangent vectors at ith vertex. If A contains the poles, they have to be dug out by deforming the contour and each pole contributes $+1$ to G_s. When C is closed, by Stoke's theorem,

$$G_s = \frac{1}{2\pi}\left[\int_C \kappa_g\, ds + \sum_i (\Delta\tau)_i + \Omega_A\right], \tag{8}$$

where Ω_A is the area of the excursion regions. This is just the Gauss-Bonnet formula for a curve on a sphere identifying G_s as the EPC χ of the excursion domain.

If L_i's are geodesic lines, κ_g vanishes and

$$G_s = \frac{1}{2\pi}\left[\sum_i (\Delta\tau)_i + \Omega_A\right]. \tag{9}$$

We note that the genus G_s as defined above is equivalent to the negative of the genus of the high-density excursion region seen in three dimensions confined to a thin spherical shell (as defined in Gott, Melott, and Dickinson 1986). In three dimensions the genus of the surface containing the high-density region is (GMD) $G_s = -(4\pi)^{-1}\int K\, dA$ where K is the Gaussian curvature. The geodesic edges are part of great circles so these are flat faces of width ϵ which have no Gaussian curvature. The curvature due to the inner and outer edges themselves are equal and opposite and so cancel out. The integrated curvature at the vertices is the angle deficit equal to the exterior angle $(\Delta\tau)_i$ and they occur in pairs, one on the outer surface of the shell and other on the inner surface, giving a total contribution $K\, dA = 2\sum_i (\Delta\tau)_i$. Finally the contribution from the outer and inner surfaces is $2\Omega_A$. Thus the three-dimensional genus of the high-density region is $G_s = -(4\pi)^{-1}[2\Omega_A + 2\sum_i (\Delta\tau)_i]$, and with a change of sign (convention) we get equation (9) directly.

Since there is no global mapping from a sphere onto a plane which not only keeps the geodesics straight but preserves the vertex angles, the evaluation of G_s seems to be nontrivial. But there is an easy way. Consider a pixeled equatorial Mercator map which is a conformal mapping of a sphere (minus the poles) onto a plane. In the equatorial Mercator map the longitude and latitude lines are straight and intersect at right angles. Equation (7) says that a longitude line segment which has $\kappa_g = 0$ (i.e., a geodesic) and $\phi =$ constant, should give no contribution to G_s, which is satisfied because it appears straight in the Mercator map. From equation (6) the latitude lines ($\tau =$ constant) have geodesic curvatures $\kappa_g\, ds = \cos(\theta) d\phi$ which also makes the integrals vanish in equation (7) so they give no contribution to G_s which is satisfied because these lines also appear straight in the Mercator map. The angles $(\Delta\tau)_i$ between neighboring contour sections are preserved because the map is conformal. Therefore for an equatorial Mercator map, equation (7) reduces to the formula of the genus for plane curves (eq. [4]). Now suppose a pole is inside an excursion region. Whether the Mercator map reaches into the excursion region or not, the genus from the Mercator map does not count it. We have to add one to the genus. If the pole temperature is below the threshold, it does not need any correction. Thus the genus for the excursions on the sky is finally

$$G_s = \frac{1}{2\pi}\sum_i (\Delta\tau)_i + N_{P(A)}\,, \tag{10}$$

where $(\Delta\tau)_i$ is now the angle between two neighboring straight

lines forming the contours in the pixeled Mercator map and $N_{P(A)}$ is the number of poles above the threshold.

An example should prove illuminating. Let the high-density region be the cap for which $\theta < \theta_0$ where $\pi/2 < \theta_0 < \pi$. Now in three dimensions this is a bowl-shaped thin shell which is one isolated high-density region, so with the sign change from GMD we expect the answer $G_s = 1$ (i.e., one isolated high-density region with no holes). Since its boundary satisfies $\kappa_s ds = \cos(\theta) d\phi$ (eq. [6]), $(\Delta\tau)_i = 0$, and the region contains one pole, we find $G_s = 1$ from equation (7). Now on the Mercator map the boundary $\theta = \theta_0$ is a straight line, so $\sum_i (\Delta\tau)_i = 0$ and the number of poles in the high-density region $N_{P(A)} = 1$, so again $G_s = 1$ from equation (10). Now rotate the sphere so that the point $\theta = 0$ is on the equator. On the Mercator map the low-density region now appears as isolated giving $(2\pi)^{-1} \sum_i (\Delta\tau)_i = -1$ and $N_{P(A)} = 2$ so $G_s = 1$ again from equation (10) showing as expected that G_s is independent of coordinate transformations.

III. EXPECTATIONS FOR GAUSSIAN FIELDS

In this section expectation values of the topological measures will be summarized for Gaussian temperature and gradient fields. Consider a Gaussian random temperature field on a two-dimensional surface parameterized by (x, y) locally. Let $C(r) = \langle (\Delta T/T)_0 (\Delta T/T)_r \rangle$ be the correlation function of the temperature fluctuations and $C_0 = C(0) \equiv \sigma^2$, where σ is the standard deviation of the temperature fluctuations, $C_2 = -(d^2C/dr^2)_{r=0}$, and $C_4 = (d^4C/dr^4)_{r=0}$ with $r = (x^2 + y^2)^{1/2}$.

The mean fractional area of excursion regions is the cumulative probability above a threshold level. For the temperature field, it is

$$\langle a \rangle = \int_\nu^\infty \frac{1}{\sqrt{2\pi}} e^{-\nu^2/2} d\nu = \frac{1}{2} \operatorname{erfc}\left(\frac{\nu}{\sqrt{2}}\right),$$

where ν is the number of standard deviations $\sigma = (C_0)^{1/2}$ above the mean and erfc (x) is the complementary error function. For one-dimensional gradient fields which are also assumed to have the Gaussian probability distribution it has the same form with a different scale factor $(C_2)^{1/2}$.

Instead of using the area fraction as a topological parameter, we are going to use it as a threshold level. Contours are thus to be defined by the fractional area f occupied by the high-temperature or high-gradient regions. We define a new label ν_A by

$$f = \frac{1}{2} \operatorname{erfc}\left(\frac{\nu_A}{\sqrt{2}}\right). \tag{11}$$

The threshold $\nu_A = 0$ divides the map into high and low regions of equal area, $\nu_A = 1$ contours enclose the excursion regions occupying 16% of the area and so on. If the field is Gaussian, ν_A is equal to ν. The benefits of using ν_A are the following: for a given sample map with unknown correlation function we do not have to know the scale factors $(C_0)^{1/2}$ or $(C_2)^{1/2}$ from the beginning, and for a non-Gaussian field the area fraction still has a meaning as a threshold level while the standard deviation becomes less meaningful.

The mean contour length per unit area has been derived by Longuet-Higgins (1957) for a general Gaussian field. For a temperature field which is assumed to be isotropic,

$$\langle s \rangle = \frac{1}{2} \left(\frac{C_2}{C_0}\right)^{1/2} e^{-\nu^2/2}, \tag{12}$$

and for the gradient field we have

$$\langle s \rangle = \frac{1}{\pi} E\left(\sqrt{\frac{2}{3}}\right) \left(\frac{C_4}{C_2}\right)^{1/2} e^{-\nu^2/2} \simeq 0.403 \left(\frac{C_4}{C_2}\right)^{1/2} e^{-\nu^2/2}, \tag{13}$$

where $E(k)$ is the complete elliptic integral of the second kind and the scale factor for ν is $(C_2)^{1/2}$.

Mean genus per unit area g is the same as the mean IGC Γ (Adler 1981) because they are essentially the expectation value of the number of excursion regions minus the number of holes in them: for the temperature field it is

$$g = \frac{1}{(2\pi)^{3/2}} \frac{C_2}{C_0} \nu e^{-\nu^2/2} \tag{14}$$

(Adler 1981; Coles 1988; Melott *et al.* 1989). This is the expectation value of the curvature integration along the contours per unit area divided by 2π.

For the one-dimensional gradient field which is anisotropic, we arrive at a formula for the mean genus per unit area with scale factor $(C_2)^{1/2}$

$$g = \frac{1}{\sqrt{3}(2\pi)^{3/2}} \frac{C_4}{C_2} \nu e^{-\nu^2/2}. \tag{15}$$

Since the curvature was calculated with respect to locally straight lines, the above formulae for g show the contribution from geodesic curvature and vertex angles. Therefore for contours on a sphere the expectation value of the total genus is (from eqs. [9] and [11])

$$G_s = 4\pi g + \operatorname{erfc}\left(\frac{\nu}{\sqrt{2}}\right), \tag{16}$$

where r in the definitions of C_0 and C_2 is measured in radians. The first term in equation (16) is equal to the first term in equation (10) for the Mercator map and the second term is the expectation value of the second term $N_{P(A)}$.

IV. APPLICATIONS TO SIMULATED MBR MAPS

In the present section we produce simulated MBR anisotropy maps with realistic power spectra and measure the topological parameters considered in the previous sections. The probabilistic behavior of those topology measures is studied for the sake of hypothesis tests on power spectra or on normality. First we shall study the Gaussian field because it is that expected in the standard model. We then analyze the MBR anisotropy map produced by cosmic strings as an example of a non-Gaussian field. For a random Gaussian field, the total contour length versus threshold and genus versus threshold curves keep their own forms and change only in amplitude for different correlation functions or power spectra. The curves have different amplitudes and shapes for a non-Gaussian field.

a) Gaussian Field

Suppose the anisotropy in the MBR is dominated by the Sachs-Wolfe effect on large angular scales ($\theta > 2°$) and by adiabatic temperature fluctuations and Doppler shifts caused by bulk motions in the last scattering shell on small angular scales and has a primordial Zel'dovich spectrum as expected in inflationary models (Bardeen, Steinhardt, and Turner 1983; Starobinskii 1982). Then, for a wide class of models with $\Omega = 1$ and adiabatic initial perturbations, the correlation function is given by (Peebles 1982; Bond and Efstathiou 1984; Vittorio and

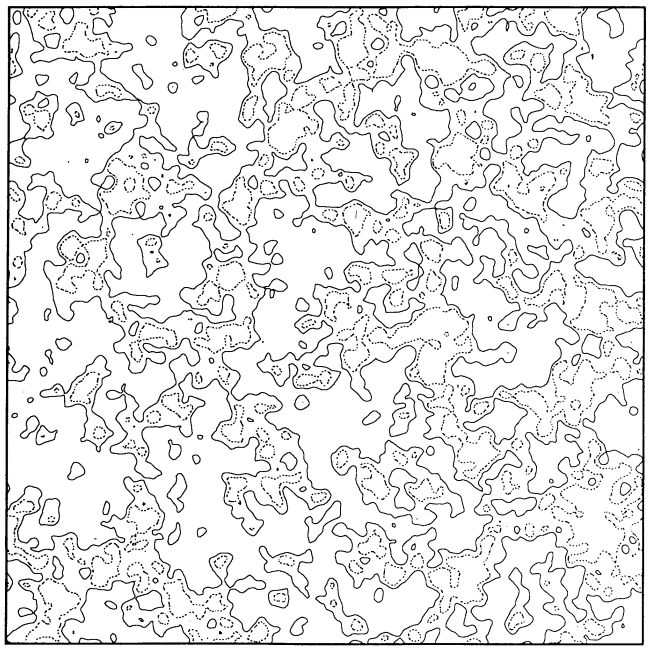

FIG. 2.—A 10° × 10° map of Gaussian MBR fluctuations having the correlation function given by eq. (17) with $\alpha = 8'$. $\nu = 0$ (*solid lines*) and 1 (*dotted lines*).

Juszkiewicz 1987)

$$C(\theta) = -\frac{3a_2^2}{\pi}\left\{\ln\left[\sin\left(\frac{\theta}{2}\right)\right] + 0.5 + 0.75\cos(\theta)\right\} \quad \text{for } \theta > 2^\circ, \quad (17)$$

$$= \frac{C(0)}{1 + \theta^2/2\alpha^2}, \quad \text{for } \theta < 2^\circ,$$

where a_2 is the rms quadrupole moment of temperature fluctuation, $C(0)$ is adjusted to produce continuity at $\theta = 2^\circ$, α is the angular scale corresponding to the thickness of the last scattering shell, and the dipole moment has been subtracted out.

We generate 10° × 10° realizations of MBR fluctuation using above correlation function with $\alpha = 8'$. Figure 2 shows the contour maps of a realization with threshold values of mean and 1 σ high. Note for a Gaussian field using the label ν is equivalent to use ν_A. The high level excursions are well isolated and have simple geometry while the mean contour is very complicated, it runs all over the survey area and ends up by crossing the boundaries. To investigate the probabilistic behavior of the topology measures we have produced 2000 simulated MBR maps on a 256 × 256 grid with the above correlation function. For each realization we measure the total contour length and the genus at 13 threshold levels from $-3\ \sigma$ to $3\ \sigma$ with a step of $0.5\ \sigma$. The method we use is as follows. We look at each of the 256 × 256 pixels on a map to find an excursion above the given threshold level. If the level is crossed within a pixel, we define an oriented line segment as a part of isotemperature contours by using x-directional and y-directional temperature gradients calculated from nearby pixels. After we define all line segments within those pixels where excursions happen, we connect the line segments that belong to a same contour. Total contour length is found by simply adding the length of each line segment. The genus comes from the sum of the exterior angles at the vertices of the contours (eq. [6]) because the contours are approximated by line segments having zero curvatures.

Figure 3*a* shows the mean genuses (*filled circles*) averaged over 2000 realizations at 13 threshold levels and the error bars denoting the $\pm 1\ \sigma$ run-to-run variations. The solid curve is the theoretical genus curve expected from equation (14). In Figure 3*b* the average contour length (*filled circles*), their $\pm 1\ \sigma$ run-to-run variations (*error bars*), and the theoretical curve (*solid curve*) expected by equation (12) are plotted. Because of the approximation of contours by line segments, the measured

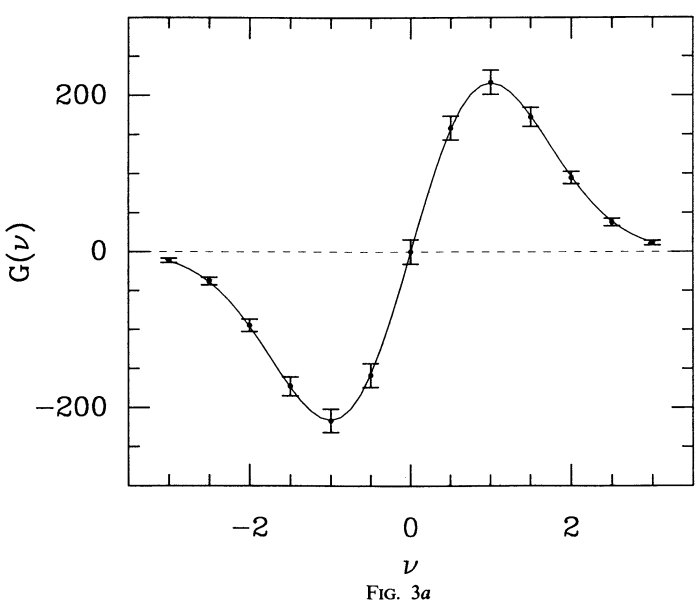

FIG. 3*a*

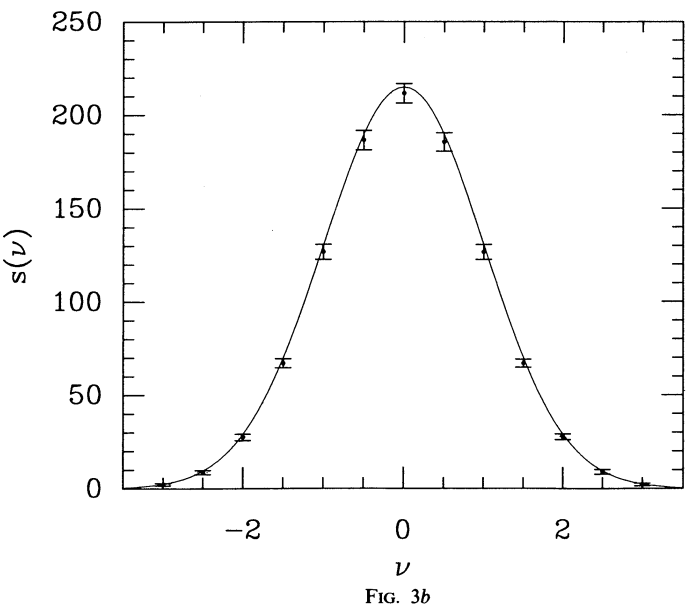

FIG. 3*b*

FIG. 3.—(*a*) The mean genuses (*filled circles*) averaged over 2000 realizations and their $\pm 1\ \sigma$ run-to-run variations at 13 threshold levels. The solid curve is the theoretical curve expected from eq. (20). (*b*) The mean contour lengths in radians per steradian (*filled circles*) and their $\pm 1\ \sigma$ run-to-run variations from the same realizations. The theoretical curve (*solid curve*) expected by equation (12) is plotted.

contour length is slightly less ($\sim 7\%$) than the theoretical value. In general, the measured genuses and total contour lengths match well with the predicted values over the entire temperature range. This allows us to analyze a map of MBR fluctuations not only at high threshold levels (Bond and Efstathiou 1987; Vittorio and Juszkiewicz 1987) but also at low thresholds for which interesting topological properties of the field appear (Coles and Barrow 1987).

It is interesting to know the probability distribution (p.d. hereafter) of the topology measures at each threshold level. Some of the existing results on the distributional behavior of excursion characteristics are the analytic formula for the moments of the number of one-dimensional level-crossings for a Gaussian process (Leadbetter and Cryer 1965; Cramer and Leadbetter 1965) and the asymptotic results on the level crossing statistic under special conditions (Adler 1981, p. 69 and the references therein).

We have determined the p.d. of the genus and the total contour length from the above 2000 simulations. Figure 4 shows the histograms of the genus and their best fitting Gaussian curves (*dotted line*) at the thresholds $\nu = 0$, 1, and 2. They are very close to Gaussian (the histogram for $\nu = 3$ just starts to deviate from the Gaussian). The distribution of total contour length is found to have the same properties. We conclude that the p.d. of the topology measures we are considering are Gaussian, and the mean and standard deviation are enough to characterize them at threshold levels for which there are many (>10) excursion regions on the map. This is in analogy with the asymptotic result (central limit theorem) for the number of zero-crossings which states that it has a normal distribution as the interval becomes large (Adler 1981, p. 69).

A more difficult problem is to find the joint p.d. of the genus or total contour length at many threshold levels, which is needed to do a goodness-of-fit test because we have to compare a sample map with the assumed model over a large temperature range. We have calculated the covariance of the genuses at threshold levels separated by 0.5 σ and found they

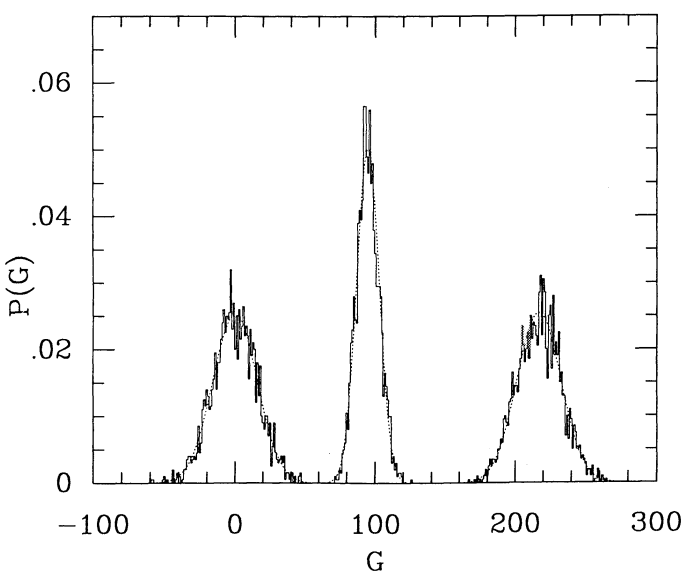

FIG. 4.—The probability distributions of the genus found from 2000 realizations of MBR maps and their best fitting Gaussian curves (*dotted lines*) at the threshold levels $\nu = 0$ (centered at $G = 0$), 1 (centered at $G = 217$), and 2 (centered at $G = 95$).

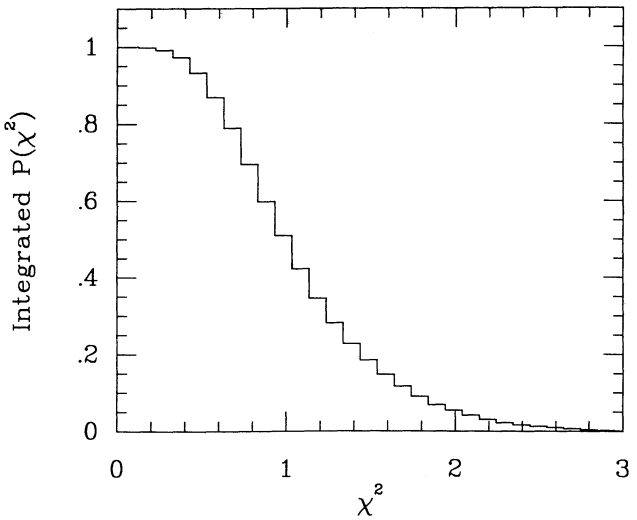

FIG. 5.—The integrated probability of χ^2 for the Gaussian maps which is defined in the text (eq. [18]).

are positively correlated with others at different threshold levels except at the level $\nu = 0$. The genus at the mean level is not correlated with the values at nearby thresholds. Therefore, the joint p.d. is not a simple multiplication of the p.d.'s at different levels. Since finding the joint p.d. is not easy even numerically, we adopt the following method. From each map we calculate the normalized χ^2 at 13 threshold levels from the definition:

$$\chi^2 = \frac{1}{12} \sum_{i=1}^{13} \frac{(G_i - \bar{G}_i)^2}{\sigma_i^2}, \tag{18}$$

where G_i is the genus measured from the map at ith level, $\bar{G}_i$ and σ_i are the mean genus and the standard deviation at that level. The degree of freedom is reduced by one because the mean genus curve has one fitting parameter, the amplitude. In Figure 5 we plot the integrated p.d. as a function of χ^2. For example, the probability of χ^2 exceeding 2 is 0.05 and of exceeding 2.6 is 0.01. Thus if a Gaussian sample map has χ^2 value greater than 2.6, we conclude it is inconsistent with the assumed model at the 99% confidence level (i.e., it has the wrong power spectrum). To test the normality of a given map we first adjust the parameter α in the correlation function (note $C_2/C_0 = \alpha^{-2}$ in eq. [14]) until the ampllitude of the Gaussian genus curve gives a best fit to the curve from the given map. With that α we find the p.d. of χ^2 from a large simulation of Gaussian maps, which enables us to test the sample map for normality.

Figure 6 shows one-dimensional gradient maps of the temperature map shown in Figure 2. They have $2(3)^{1/2}$ times more structures (eqs. [14] and [15]) than the temperature map and their structures are typically elongated toward the direction perpendicular to the gradient vector. The genus and total contour length for the gradient field have similar probabilistic behavior to those for the temperature field. For example, we plot the genuses and total contour lengths of the x-gradient field, their ± 1 σ range of run-to-run variations (error bars) from 100 realizations, and the best fitting theoretical curve given by equations (15) and (13) (*solid curve*) in Figures 7*a* and 7*b*. The amplitudes of those curves are again less than the theoretical values due to the smoothing effect of the finite size

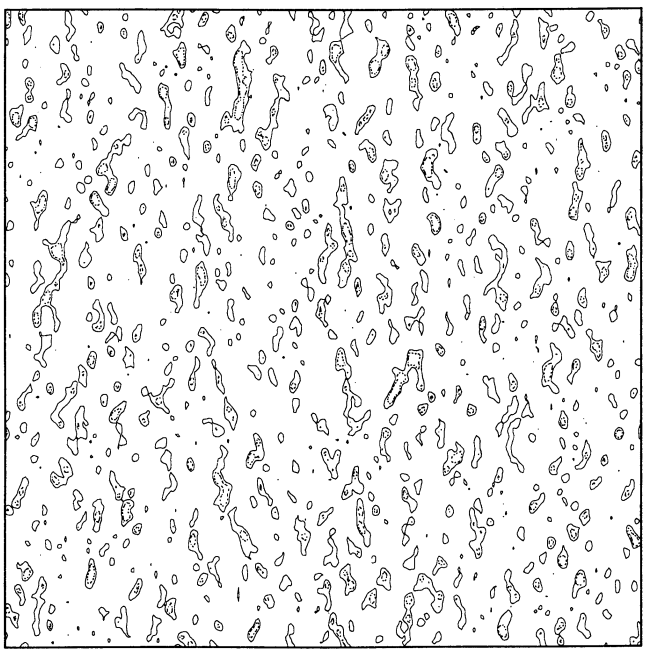

FIG. 6a

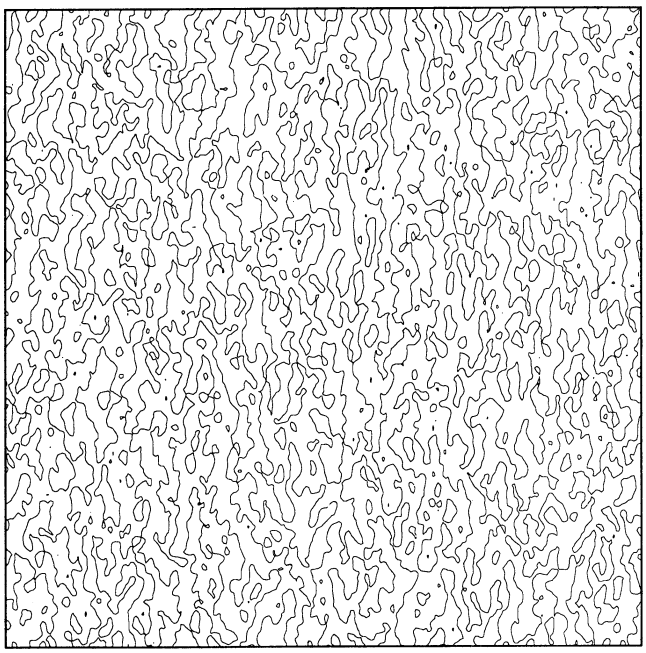

FIG. 6b

FIG. 6.—Maps of the x-component of the temperature gradient of a Gaussian MBR map. (*a*) $\nu = 1$ (*solid lines*) and 2 (*dotted lines*). (*b*) $\nu = 0$.

pixels. Convergence to the theoretical amplitude has been checked for these maps with 512 × 512 and 1024 × 1024 grids.

As an example of Gaussian random field on the sphere we generate the MBR fluctuation pattern (without the dipole term) over the entire sky by using a spherical harmonic expansion of the radiation anisotropy

$$\frac{\delta T}{T_b} = \sum_{l=2}^{l_{\max}} \sum_{m=-l}^{l} a_l^m Y_l^m(\theta, \phi) , \tag{19}$$

where the a_l^m's are Gaussian random variables with zero means and standard deviations equal to $[P(l)]^{1/2}$. For the Zel'dovich scale-free power spectrum of density fluctuations, the power spectrum of the expansion coefficients a_l^m (calculated from the Sachs-Wolfe effect for scales $> 2°$) are given by (Peebles 1982)

$$P(l) = \langle |a_l|^2 \rangle \propto \frac{1}{l(l+1)} . \tag{20}$$

If we use a symmetric beam for observation, the beam profile can be decomposed as

$$F(\theta) = \sum_l \frac{2l+1}{4\pi} F_l P_l(\cos\theta) .$$

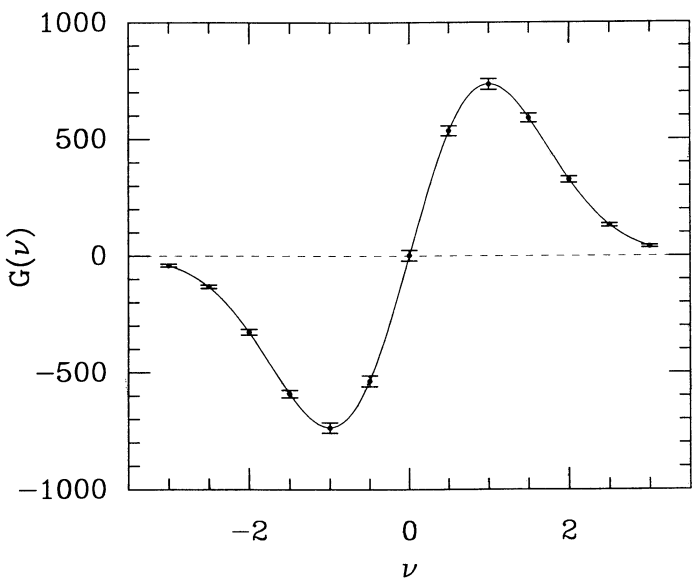

FIG. 7a

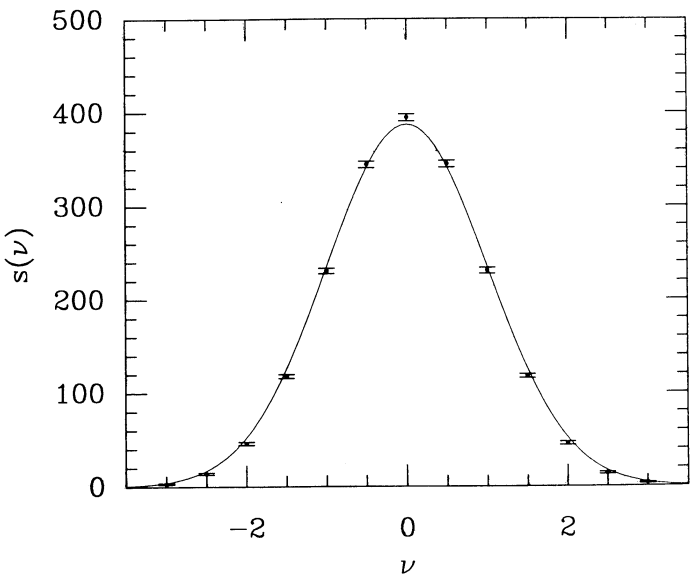

FIG. 7b

FIG. 7.—The genus (*a*) and the total contour length in radians per steradian (*b*) averaged over 100 x-gradient maps, their $\pm 1\ \sigma$ range of run-to-run variations (*error bars*), and their theoretical curves.

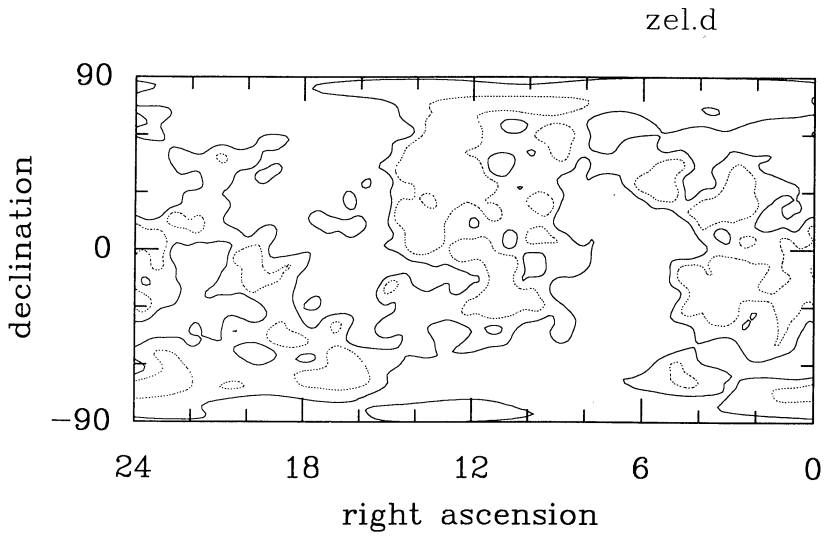

FIG. 8*a*

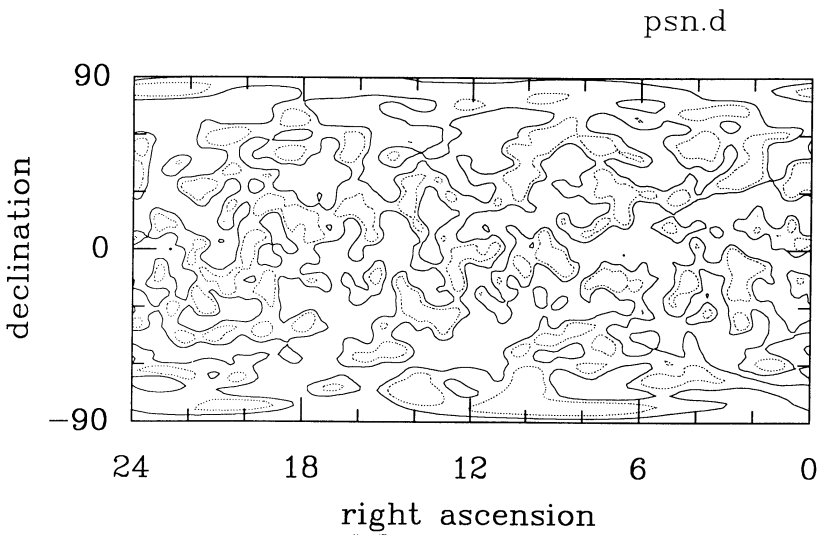

FIG. 8*b*

FIG. 8.—A whole sky map of MBR anisotropy smoothed by a Gaussian beam with FWHM = 7° (the same resolution as COBE). The solid lines are the mean levels and the dotted ones are $\nu = 1$ contours. (*a*) A map with Zel'dovich power spectrum. (*b*) A map with Poisson power spectrum. This map mimics a MBR experiment dominated by noise.

If $F(\theta)$ is Gaussian with smoothing angle θ_s, i.e., $F(\theta) = (2\pi\theta_s^2)^{-1} \exp(-\theta^2/2\theta_s^2)$, the F_l are given by (Scaramella and Vittorio 1988)

$$F_l = e^{-\theta_S^2(l+1/2)^2/2} .$$

The convolved temperature fluctuation is simply

$$\frac{\delta T}{T_b} = \sum_{l=2}^{l_{\max}} \sum_{m=-l}^{l} a_l^m F_l Y_l^m(\theta, \phi) , \qquad (21)$$

where $l_{\max}$ is a sufficiently large number such that $a_{l_{\max}} F_{l_{\max}}/a_2 F_2 \ll 1$.

A whole sky contour map is given for a Zel'dovich power spectrum with $\theta_s = 3.^\circ 5$ (FWHM = 7°) in Figure 8*a* and various map projections of the Zel'dovich map with no smoothing but $l_{\max} = 90$ (effective smoothing length of 2°) are shown in Figure 9 (Plates 1–2). In Figure 8*b* we used a Poisson power spectrum $P(l) =$ constant and the same smoothing angle intending to mimic instrumental noise. Obviously the Zel'dovich map has fewer small-scale structures and more large-scale structures compared to the Poisson map because it has more power on large scales than white noise. The actual map we get from an observation is the superposition of a real signal distribution convolved with the beam pattern plus a noise map smoothed over sampling interval. Both the Zel'dovich and the noise maps are random Gaussian, so the genus curve of the Zel'dovich map has the same shape but different amplitude compared to that of a noise map. Therefore in this case we can test the hypothesis of a real signal against the alternative that there is only instrumental noise by estimating the probability of χ^2 of a simulated noise map exceeding the value measured from the observed map. The method of normality test is similar to that described above. Figure 10 shows how well the genus curves with Zel'dovich and Poisson spectra are separated. As the signal-to-noise ratio increases, the observed map will start to depart from the Poisson curve, and we can detect the signal at a certain con-

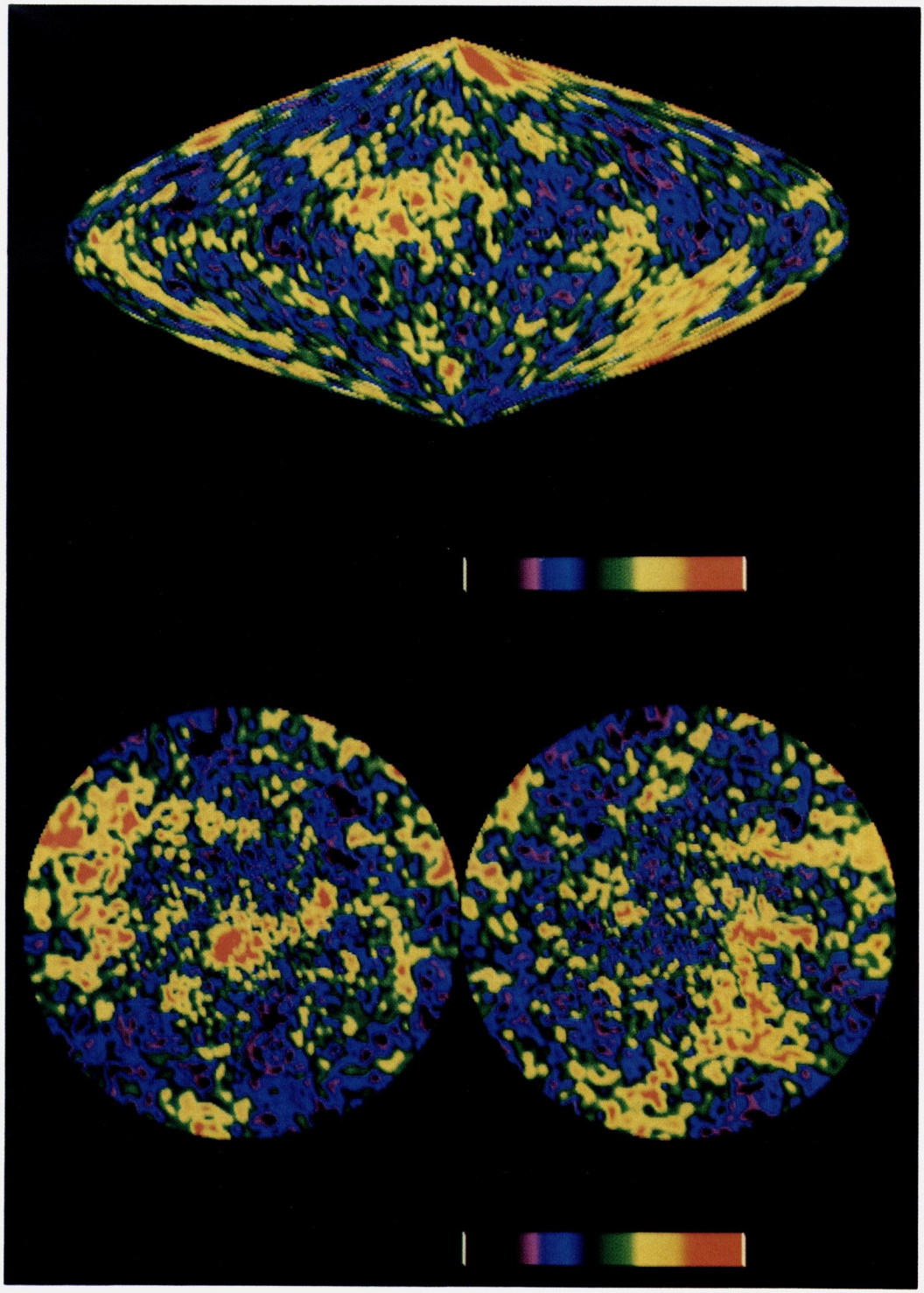

FIG. 9*a*

FIG. 9.—(*a*) Whole sky maps of MBR anisotropy with a Zel'dovich power spectrum with an effective resolution of 2° (3.5 times better resolution than COBE). Color bars show fluctuations from $-3\,\sigma$ to $+3\,\sigma$ on a linear scale. *Top:* sinusoidal equal area projection. *Bottom:* steriographic projections of northern and southern hemispheres.

GOTT *et al.* (*see* **352**, 8)

PLATE 2

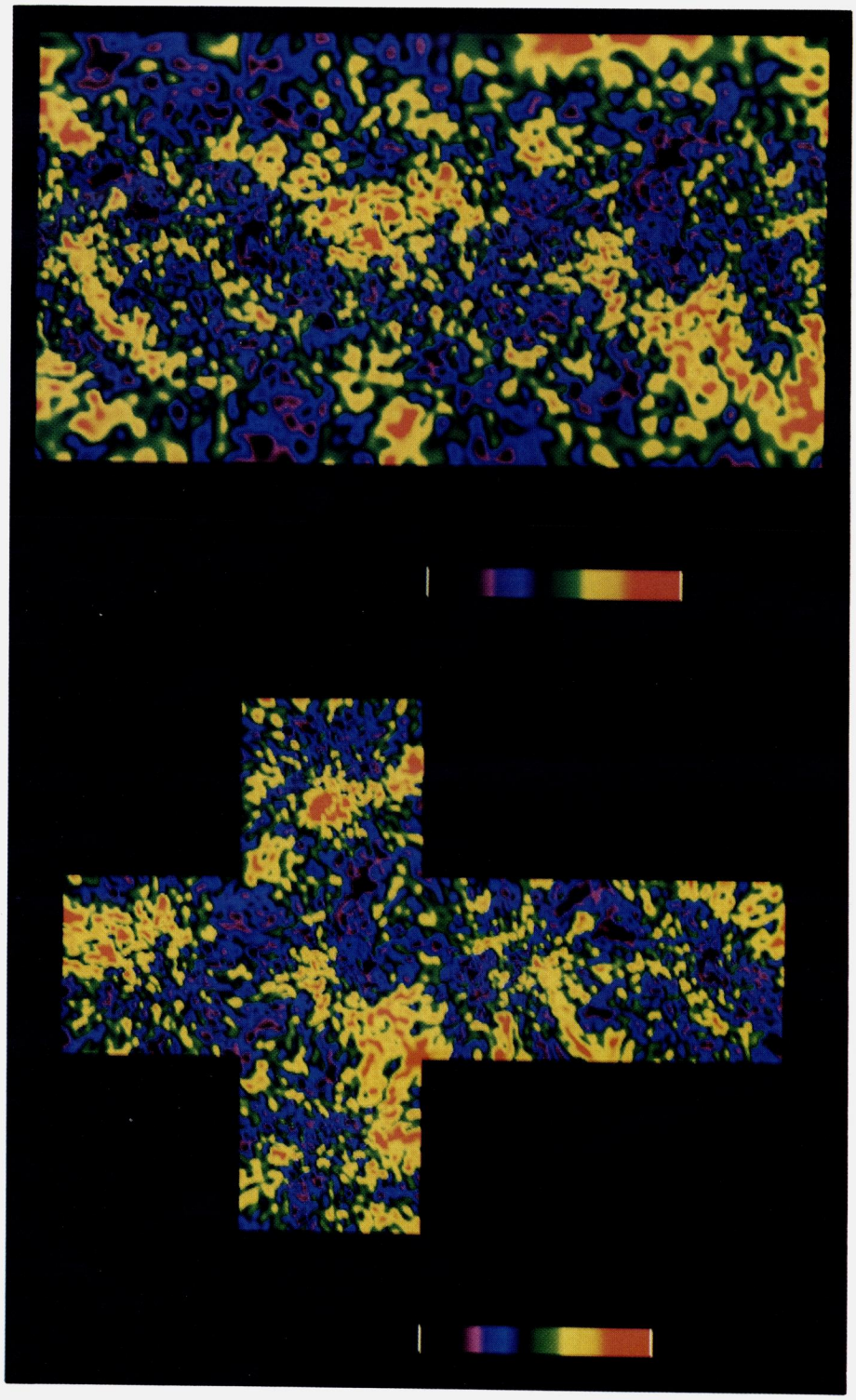

FIG. 9b

FIG. 9.—(*b*) Whole-sky maps of the MBR anisotropy as in Fig. 9*a*. *Top:* mercator projection with the declination in the range from −70° to 70° *Bottom:* gnomonic projection on the surface of a cube.

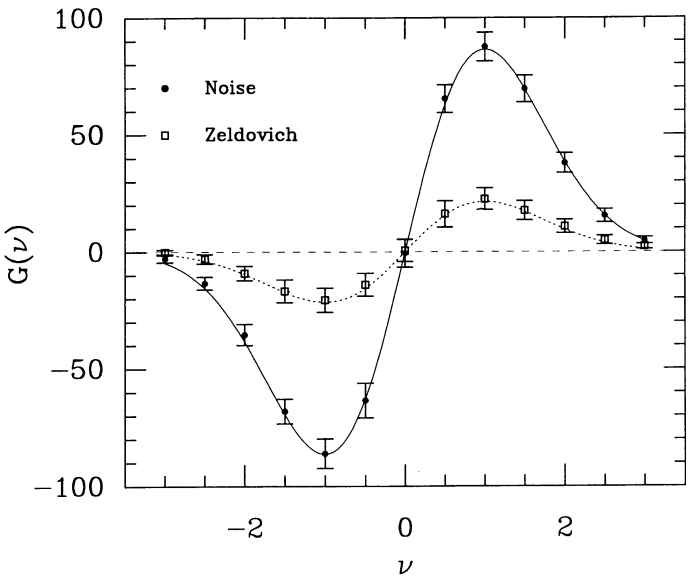

FIG. 10.—The mean genuses of the Zel'dovich and Poisson maps shown in Fig. 8 and their $\pm 1\ \sigma$ run-to-run variations over 100 realizations illustrating the difference between a MBR map with real signals and a map dominated by noise.

fidence level. In the next paper (Park and Gott 1990) we apply these techniques to analyze the Princeton and Berkeley MBR maps and deduce that for a Zel'dovich spectrum $\langle a_2^2 \rangle^{1/2} \leq 5.8 \times 10^{-5}$.

b) Non-Gaussian Field: Cosmic String Map

Moving cosmic strings produce distortions in the cosmic microwave background (Kaiser and Stebbins 1984; Gott 1985). A nearby cosmic string moving with velocity v perpendicular to the line of sight produces a discontinuity of $\Delta T/T = 8\pi G\mu v/c$ in the MBR across the string. Here we test the sensitivity of our statistics in discriminating the anisotropy patterns produced by cosmic string networks (string map hereafter) from the standard Gaussian fluctuations (Gaussian map). For details of the numerical simulation of cosmic string evolution and the resultant MBR pattern see Bouchet, Bennet, and Stebbins (1988).

Figure 11*a* shows the contour plot of the temperature fluctuations of the string map which has $(\Delta T/T)_{\rm rms} = 17G\mu$ on 256 × 256 grid (Bouchet, Bennet, and Stebbins, 1988, Fig. 1). Its angular size is 7°.2 × 7°.2 assuming the epoch z_s of last scattering is equal to ~1000. The statistical property of a map we tend to consider first as a discriminator would be the temperature histogram. As Figure 12*a* shows, however, the temperature histogram of the string map does not show a large deviation from the Gaussian curve. In fact, the string map has many high-σ fluctuations; there are ~10 pixels which have temperature values above 5 σ while we expect 0.02 pixel for a Gaussian field. However, in a realistic observational situation very high σ fluctuations are usually dominated by observational shot noise or by unresolved point sources, and it is very dangerous to draw conclusions based on several pixels on the map.

We next consider the histogram of the temperature gradient field. Figure 11*b* is a contour plot showing 1 σ high levels of x-gradient field of the string map. Figure 12*b* demonstrates clearly the non-Gaussian behavior of the string gradient field map. The tails of the histogram extend all the way out to 13 σ. The string segments which have large transverse velocities produce discontinuities in the temperature field, and in the gradient map they appear as very steep mountain ranges. Collapsing string loops and crossing networks also produce strong peaks in the gradient map. On the other hand, the regions bounded by strings have flat temperature distributions which

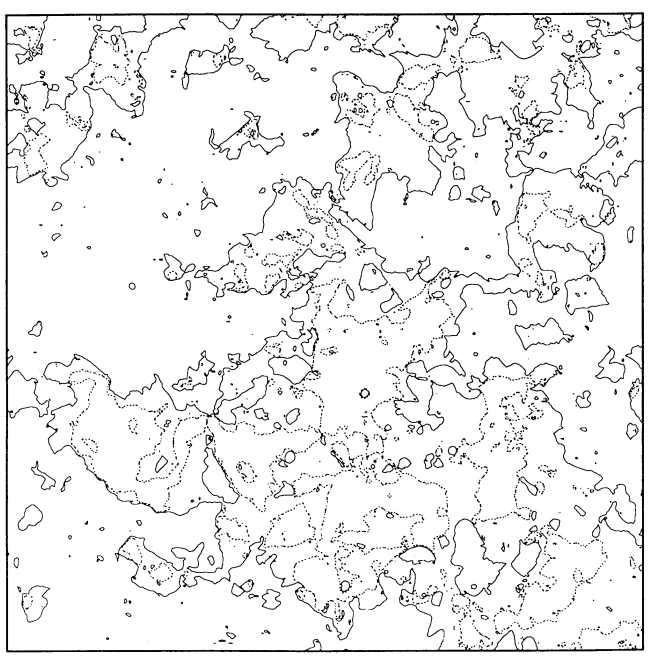

FIG. 11*a*

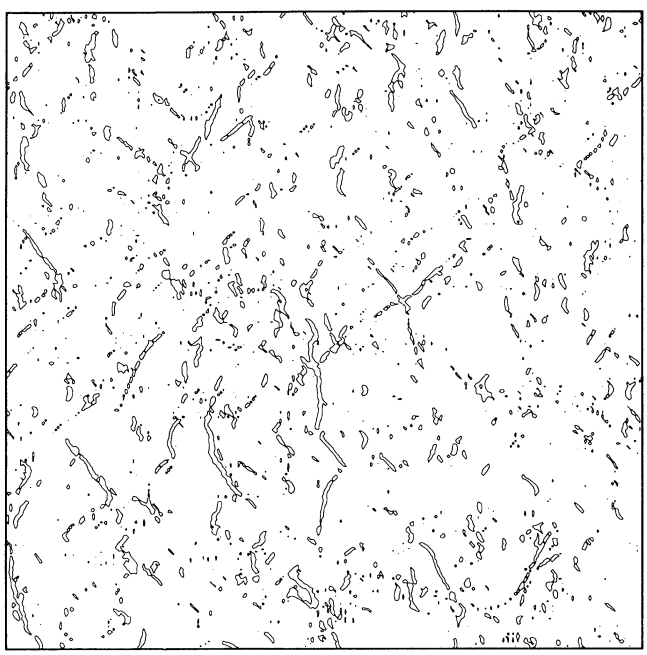

FIG. 11*b*

FIG. 11.—(*a*) Simulated MBR anisotropy pattern due to cosmic string networks. The map size is ~7°.2 × 7°.2. Solid lines denote the $\nu = 0$ contour level and dotted lines the $\nu = 1$ high level. (*b*) $\nu = +1.4$ contours of x-component of temperature gradient field of the string map.

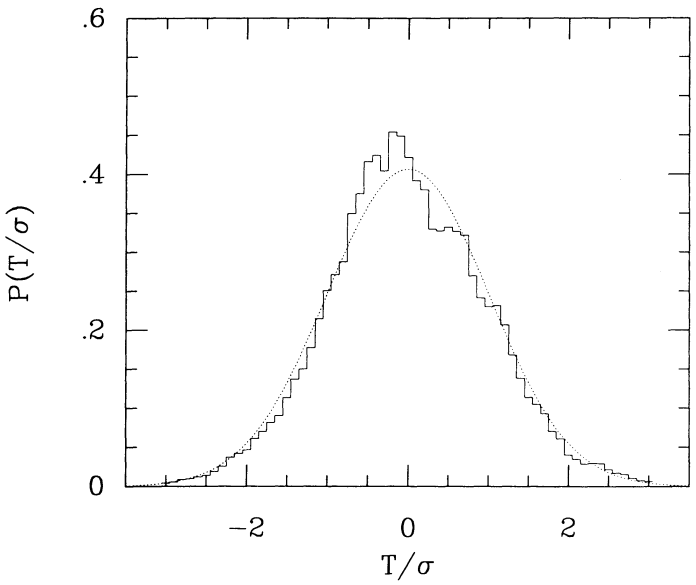

FIG. 12*a*

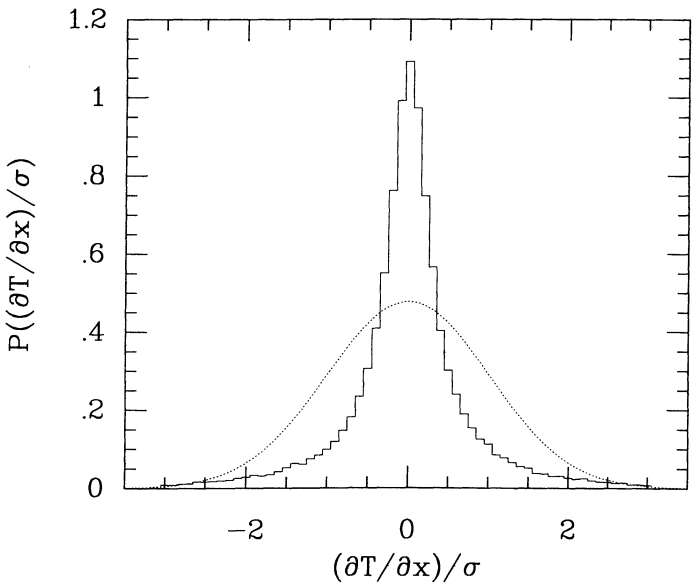

FIG. 12*b*

FIG. 12.—Histograms of (*a*) temperature and (*b*) *x*-component of temperature gradient fields of the string map. Each field is scaled in units of its rms fluctuation σ.

have very small gradients. The remarkable deviation of the gradient histogram from the Gaussian curve is, therefore, an intrinsic geometrical property of the MBR anisotropy pattern produced by cosmic strings.

In order to see the sensitivity of the gradient histogram to the presence of a stringy temperature fluctuation, a χ^2-test has been done to the composite maps of the string and the standard Gaussian (with $\alpha = 8'$) map. The probability distribution of χ^2 which has a definition similar to equation (18), is found from the gradient histograms of 500 realizations of the Gaussian maps with the correlation function given by equation (17). We prepare a composite map by adding the normalized string map to the Gaussian map, and the χ^2 value of its gradient histogram from the mean gradient histogram of the Gaussian maps is calculated. When the string map fraction f_s (i.e., the rms amplitude of the string map relative to that of the Gaussian map) becomes larger than 0.47, the probability of χ^2 of a Gaussian map exceeding the value of the composite map falls below 1%. Only the part of the histogram within $\pm 3\ \sigma$ has been taken into consideration in this test. The excees of high-σ gradient peaks cannot be simply neglected as before because they are steep cliffs on temperature maps whose coherent structures might not be easily produced by instrumental noise or by point sources. Besides the test for non-Gaussian behvior the gradient map may be used to actually locate stringy and knotty features on a MBR fluctuation map for further study (i.e., to look for gravitational lensing events; Gott 1985).

Second, we use the total contour length in order to distinguish the string map from the Gaussian one. Contour lengths measured from the string map are plotted in Figures 13*a* and 13*b* together with the best fitting theoretical curves. We see significant deviation from the Gaussian curve for the gradient field. We apply the χ^2-test we used above to the contour length of the string map. In order to recognize the non-Gaussian behavior only we first find a Gaussian map (i.e., fixing the parameter α) whose contour length curve best fits that of a composite map (string plus standard Gaussian map) and then calculate the χ^2. For the temperature field we get a critical string map fraction $f_s = 1.7$ above which the composite map becomes surely inconsistent (probability less than 0.01) with the assumed Gaussian map. We get $f_s = 0.67$ for the gradient map.

Last, we exploit the genus as the discriminator. Figures 14*a* and 14*b* show the total genus of the temperature and gradient fields of the string map and their best-fit theoretical curves (eqs. [14] and [15]). The amplitude of the theoretical curve which fits to the genus of string temperature map implies that a Gaussian field has about the same number of structures if $\alpha = 5'.2$. The composite map of Gaussian temperature field plus string temperature map fails the χ^2-test for a Gaussian field hypothesis when the fraction of string map is increased to 0.94 and the composite map becomes surely non-Gaussian ($P < 0.01$). For the genus of the gradient field we find $f_s = 0.24$; the best sensitivity to the non-Gaussian behavior of the string map. Since $(\Delta T/T)_{\rm rms} = 27\langle a_2^2\rangle^{1/2}$ for the standard Gaussian map with $\alpha = 8'$ (eq. [17]) and $17G\mu$ for the string map, the non-Gaussianity of the string network can be recognized by the technique above if

$$G\mu > 1.6 f_s \langle a_2^2\rangle^{1/2} = n_1 \langle a_2^2\rangle^{1/2}\ , \qquad (22)$$

where $n_1 = 0.73$, 2.7, 1.1, 1.5 and 0.38 for gradient histogram, total contour length of temperature and gradient fields, and genus of temperature and gradient fields, respectively

In practice, an observed map will contain instrumental noise so we perform the above tests on composite maps of size $7^\circ.2 \times 7^\circ.2$ containing Gaussian MBR fluctuations with $\alpha = 8'$ plus Gaussian instrumental noise as well as strings plus Gaussian instrumental noise in order to find the signal-to-noise ratio at which we can reject the pure noise hypothesis for the observed map. We prepare a noise map which has random Gaussian values in each pixel ($1'.7 \times 1'.7$) with a fixed standard deviation. The noise map is extremely choppy, and its genus is highly nonrandom phase due to the effect of finite pixel size (but pixel values are Gaussian distributed). From the variation of the amplitude of genus curve we find the critical fraction of Gaussian MBR map and the string map to be $f_g = 0.15$ and $f_s = 0.14$

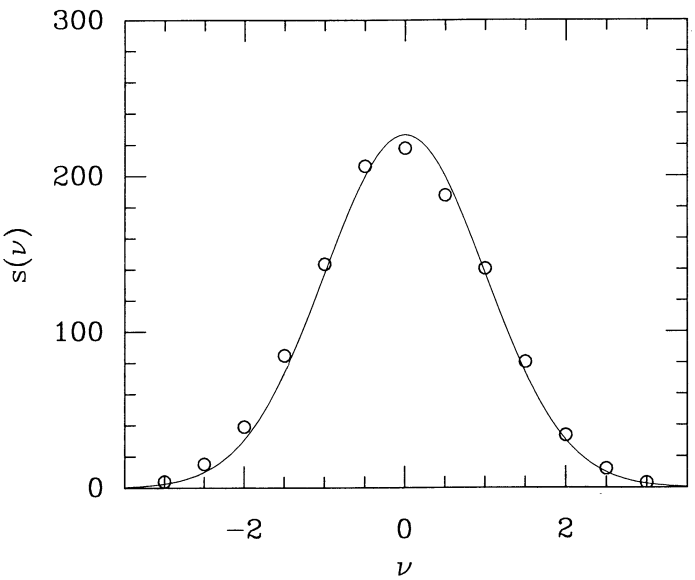

FIG. 13*a*

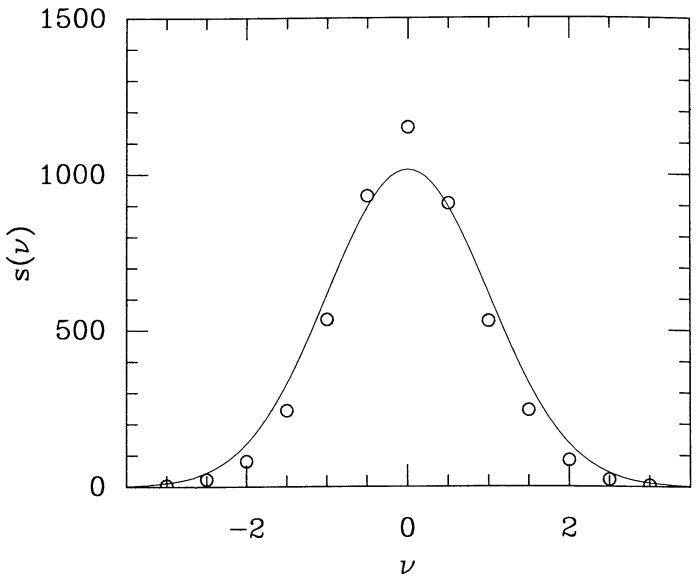

FIG. 13*b*

FIG. 13.—Contour lengths per unit area of the (*a*) temperature and (*b*) temperature gradient fields of the string map. Solid lines are best fitting Gaussian curves.

for temperature field, and $f_g = 0.51$ and $f_s = 0.6$ for gradient field. These are the signal-to-noise ratios we have to reach so that we can reject the noise hypothesis for the observed map with a 256 × 256 grid.

Specifically, if the sky has a Zel'dovich spectrum with $\langle a_2^2 \rangle^{1/2} = 1 \times 10^{-5}$ (close to the upper limit deduced by Park and Gott [1990] from a topological study of the Princeton and Berkeley all sky maps), then on a 7°.2 × 7°.2 patch of sky $(\Delta T/T)_{\rm rms} = 9.7 \times 10^{-5}$ (eq. [17]). To detect this signal with the genus technique for a temperature map with a 256 × 256 (1'.7 × 1'.7) grid would require a rms noise temperature $(\Delta T/T)_{\rm rms}$ of less than 6.5×10^{-4}. If strings with $G\mu = 10^{-6}$ were the only source of fluctuations, detecting the string signal using the genus technique for the temperature field would require a rms noise temperature $(\Delta T/T)_{\rm rms}$ less than 1.2×10^{-4}. The total observing times required to beat these limits are then given by

$$t_{\rm obs} > n_2 \left(\frac{S}{0.2 \text{ mK Hz}^{-1/2}} \right)^2 \left(\frac{10^{-5}}{\langle a_2^2 \rangle^{1/2}} \right)^2 , \qquad (23a)$$

where $n_2 = 10 f_g^2$ hr = 0.23 hr for the Gaussian MBR map and

$$t_{\rm obs} > n_2 \left(\frac{S}{0.2 \text{ mK Hz}^{-1/2}} \right)^2 \left(\frac{10^{-6}}{G\mu} \right)^2 , \qquad (23b)$$

with $n_2 = 336 f_s^2$ hours = 6.6 hr for the pure string map. S is the sensitivity of the observing system and, for example, was 5, 13, 14, and 9 mK Hz$^{-1/2}$ for the large-scale anisotropy experi-

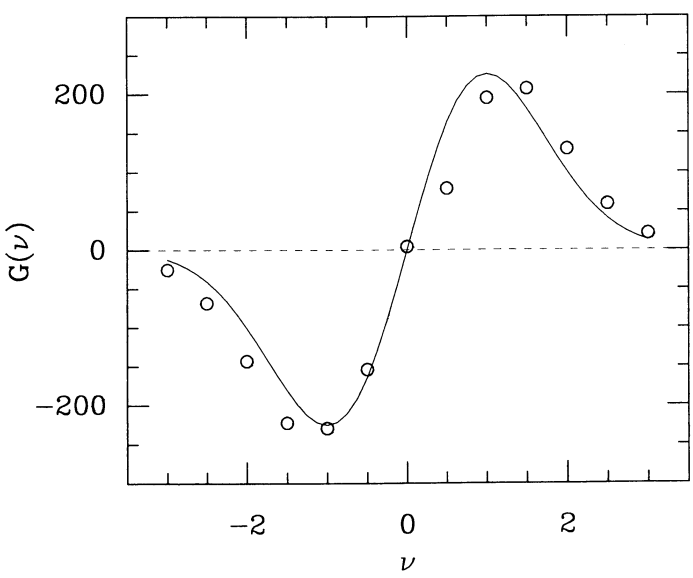

FIG. 14*a*

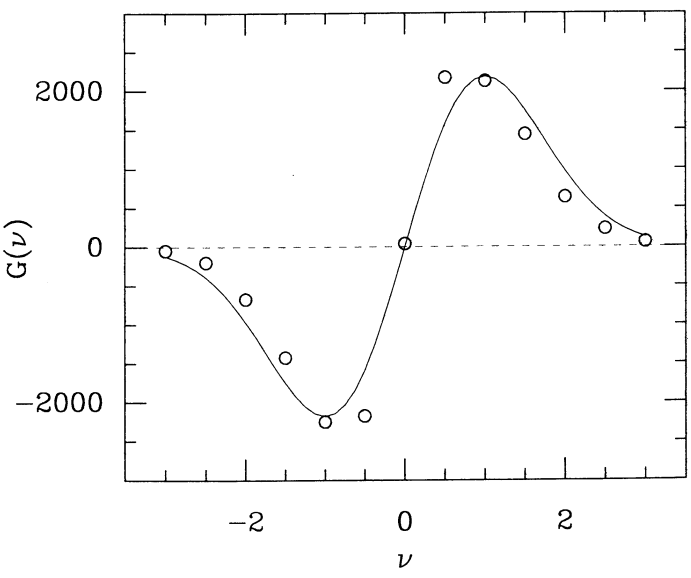

FIG. 14*b*

FIG. 14.—Total genuses of the (*a*) temperature and (*b*) *x*-component of the gradient field of the string map and their best-fit theoretical curves

ments of Fixen *et al.* (1983) and Lubin *et al.* (1985) and the small-scale experiments of Uson and Wilkinson (1984) and Readhead *et al.* (1988), respectively. Dragovan (1989), however, hopes to build a 3 mm system with a sensitivity of ~ 0.2 mK $\mathrm{Hz}^{-1/2}$.

Recognizing the non-Gaussian behavior of the string MBR fluctuation is much harder than simply detecting a signal out of instrumental noise. We consider two cases: a MBR with the string signal only and with both Zel'dovich Gaussian and string signals. For the second case we choose the parameters as $\langle a_2^2 \rangle^{1/2} = G\mu$ or $2G\mu$. We perform the non-Gaussianity test for composite maps with those signals plus Gaussian noise and find the critical signal-to-noise ratios to be 1.5, 1.6, and 1.9 for the above cases, respectively. The total observing time is given by equation (23b) with $n_2 = 336 f_{\mathrm{signal}}^2$ hr = 760, 860, and 1200 hr, respectively. If $G\mu$ becomes less than $\frac{1}{2}\langle a_2^2 \rangle^{1/2}$, the non-Gaussian behavior due to string features becomes increasingly difficult to detect.

V. SUMMARY AND DISCUSSION

Information on spatial structures is often drawn from observations in projection (i.e., angular distribution of galaxies, MBR) or sections (i.e., pencil beams and slice surveys of galaxies, and one-dimensional scans of the MBR).

Coles and Barrow (1987) and Ryden (1988) proposed that the one-dimensional level crossing statistic N_1 could give statistical information in all three dimensions, i.e., contour length in two dimensions or contour surface area in three dimensions (Ryden *et al.* 1988).

The high level excursion statistics like the average number, size, and shape of peaks (Sazhin 1985; Bond and Efstathiou 1987; Vittorio and Juszkiewicz 1987) have received great attention because the extrema are easy to detect and have simple geometry. However, peaks higher than 3 σ are very rare for Gaussian fluctuations and peak statistics are not particularly sensitive to non-Gaussian behavior of the field (Coles and Barrow 1987). Full statistical information can be drawn only when we also consider the low-level contours ($|\nu| < 3$) for which most interesting topological structures occur.

For structures in two- or three-dimensional spaces invariant quantities under Euclidean motions are the contour length (or contour surface area) and the surface curvature. In this paper we have focused on the study of two-dimensional random temperature fields. Three topological parameters: total area of the excursion regions, total length, and total curvature of the isotemperature contours or the boundaries of the excursion sets, are considered and the genus is defined as a measure of the total curvature. The genus is an ideal statistic for the study of MBR fields because (1) it is easy to evaluate for all threshold levels unlike the peak statistic, (2) it does not require the compactness of excursion regions unlike the Euler-Poincare characteristic, and (3) is independent of any rigid coordinate transformation unlike the integral geometric characteristic. Formulae for the mean value of the genus as a function of density enhancements are presented for Gaussian temperature and gradient fields. The genus of excursion regions on the curved surface of a sphere is also defined, and its expectation value is derived.

Recently Coles (1988) has used three geometric quantities to test the normality of a field: IGC, total number of up-crossings along the rows and columns of the map grid, and the mean size of the excursions, and demonstrated that the IGC is most sensitive to departures from normality. Coles also pointed out that the mean size of the excursion regions is not very sensitive to non-Gaussian behavior of a field and thus is a better statistic for estimating the statistical parameters (see also Ryden *et al.* 1989). As we pointed in § II, the value of the IGC depends on the position of survey boundaries unless they are periodic. This boundary effect becomes small when there are many structures not intercepted by boundaries. It is expected that the observed MBR map may have complicated boundaries (Fixen, Cheng, and Wilkinson 1983; Lubin *et al.* 1985; Dragovan 1989), and the measured value of the IGC might be dominated by the random error introduced by the boundary effect. On the other hand, the genus and its computation scheme depend only on the local temperature field from which contours are found, and the genus accurately represents the topological properties of a random field without boundary effects.

We generated $10^\circ \times 10^\circ$ Gaussian MBR anisotropy maps with the correlation function of the standard scenario and measured the genus and total contour length using the total area of excursion domains to define threshold levels. Their mean values are in excellent agreement with the theoretically expected values and the probability distribution at each threshold level (up to $\nu = 3$) is found to be normal for the assumed MBR fluctuation models. The effect of finite pixel size is found for both statistics, which has been studied by Melott *et al.* (1989). A simulated MBR fluctuation map produced by cosmic strings is extensively analyzed in order to prove the sensitivity of the topological measures to the existence of string features on a Gaussian background.

In order to draw conclusions for a given map, we used a normalized χ^2-test which measures the deviation of the sample's genus curve from that of an assumed model at many threshold levels. For a Gaussian field we can investigate its power spectrum by this method and for a field whose normality is suspected we can test it by comparing it with a Gaussian field having the same covariance.

The temperature gradient field is very sensitive to the fluctuations produced by cosmic strings because the discontinuities and plateaus in temperature distribution will appear as sharp peaks and zero-gradient surfaces in the gradient map. The geometric characteristics of a Gaussian gradient field are studied and several useful relations for detectability of signals and non-Gaussian behavior of string features are found.

While our examples of a Gaussian field with a Zel'dovich spectrum and non-Gaussian fluctuations from cosmic strings have allowed us to focus our attention on these specific cases, our study is by no means complete. Here we would like to outline some potentially important effects which have not been included in our simulations. First, our Gaussian example has assumed hydrogen recombination at $z = 1000$ and no subsequent reheating of the intergalactic medium (IGM). Meanwhile there are both observational (the Gunn-Peterson test) and theoretical reasons (all models with early galaxy formation) to believe that the IGM may have been reionized in the past. If this happened early enough, the anisotropy on angular scales $\theta \leq 5^\circ$ (e.g., Peebles 1987) would have been severely modified. The primeval $\Delta T/T$ generated at $z = 1000$ is erased and secondary anisotropies are generated. In gravitational instability scenarios with reheating, the dominant secondary $\Delta T/T$ is induced by bulk flows (Sunyaev 1978; Ostriker and Vishniac 1986; Vishniac 1987). The anisotropy at $\theta \geq 5^\circ$ is not sensitive to ionization history. Second, we have assumed adiabatic perturbations with a Zel'dovich spectrum and a flat universe. Although this is undoubtedly the most

"natural" outcome of inflation, other cases can be cooked-up. There are inflationary models which break scale-invariance, adiabaticity and Gaussian statistics (Kofman and Linde 1987; Grinstein and Wise 1987; Salopek, Bond, and Bardeen 1988; Peebles 1988). There are also examples of negatively curved ($\Omega < 1$) bubble universes that emerge from inflation (Gott 1982, 1986; Gott and Statler 1984). Calculating the large-scale anisotropy generated in $\Omega < 1$ models is still a problem that challenges theoretists. Apart from noticing interesting geometrical effects of curvature like Novikov's (1968) "ring of fire" (see also Bajtlik *et al.* 1986) and finding the $C(\theta)$ for some limiting cases (Wilson 1983; Peebles 1982; Gorski and Silk 1989), the problem has not yet been solved. Third, there obviously are many possible sources of non-Gaussian behavior on angular scales of several arcminutes, and our string-generated pattern is only one of these. In structure formation theories with explosions, either driven by supernovae (Ostriker and Cowie 1981; Ikeuchi 1981) or superconducting cosmic strings (Ostriker, Thompson, and Witten 1986) the MBR pattern is dominated by non-Gaussian secondary anisotropies induced by bulk flows (Sunyaev 1978) and electron scattering off a hot moving inhomogeneous gas (Vishniac 1987), or the Sunyaev-Zel'dovich (1970) effect. Finally, using Sunyaev's (1977) classification, we should mention observable sources of $\Delta T/T$, such as clusters of galaxies or radio sources. These are likely to dominate MBR maps on angular scales smaller than few arcminutes. The Sunyaev-Zel'dovich effect on the hot gas in clusters is expected to produce a significant non-Gaussian pattern (cold spots on a hot background) (Cole and Kaiser 1988) and we can also expect non-Gaussian patterns from young galaxies, radio sources, etc. However, these effects would not show up in a map made with angular resolution $\theta \geq 1°$.

Whole sky MBR maps have been produced in the past (Fixen, Cheng, and Wilkinson 1983; Lubin *et al.* 1985; Strukov, Skulachev, and Klypin 1987) without finding the quadrupole or higher moments of temperature fluctuation. For the residual temperature fluctuation with the dipole term and the galaxy contribution subtracted out of the original observation map, we can ask whether or not what is left is just instrumental noise with a power spectrum determined by the observation and reduction processes, or if a signal is present, what kind of statistical properties it has. If the signal-to-noise ratio is low, we will see temperature fluctuations dominated by noise, while we map real MBR anisotropies in the limit of infinite signal-to-noise ratio. To mimic those situations we generated whole sky maps with Poisson and Zel'dovich spectra to represent the noise and signal maps, respectively. A real observation would give a composite map with the fraction of Zel'dovich map equal to the signal-to-noise ratio if the MBR anisotropy pattern has Zel'dovich power spectrum (eq. [20]) at large angular scales. In the paper subsequent to this we apply the above method to real all-sky MBR observation maps from Princeton and Berkeley experiments and deduce that for a Zel'dovich spectrum $\langle a_2^2 \rangle^{1/2} \leq 1.2 \times 10^{-5}$ (Park and Gott 1990). Given this and equation (23b) we find that with current obseratonal sensitivity ($S = 5$ mK Hz$^{1/2}$ as in the experiment of Fixen *et al.* 1983) and a 32 receiver system (as used by Dragovan 1989) 660 hr of mapping would be required to demonstrate the non-Gaussian behavior of cosmic strings if $G\mu \geq 6 \times 10^{-6}$. If such an observational program failed to detect any signals beyond instrumental noise we would be able to set limits (using eq. [23]) of $G\mu \leq 4 \times 10^{-7}$ and for a Zel'dovich spectrum $\langle a_2^2 \rangle^{1/2} \leq 8 \times 10^{-7}$.

We wish to acknowledge support from NSF grant AST 87-21484 (J. R. G.) and from NASA astrophysical theory grant NAGW-765 (J. R. G. and D. P. B.). R. J. acknowledges support from New Jersey High Technology Grant 88-240090-2. The work of D.P.B. was also supported by NSF grant PHY 80-19725. F. R. B. was supported in part by the Theoretical Astrophysics Center at the University of California at Berkeley, and under the auspices of the US Department of Energy by Lawrence Livermore National Laboratory under contract No. W-7405-Eng-48.

REFERENCES

Adler, R. J. 1981, *The Geometry of Random Fields* (New York: Wiley).
Bajtlik, S., Juszkiewicz, R., Proszynski, M., and Amsterdamski, P. 1986, *Ap. J.*, **300**, 463.
Bardeen, J. M., Bond, J. R., Kaiser, N., and Szalay, A. S. 1986, *Ap. J.*, **304**, 15.
Bardeen, J. M., Steinhardt, P. J., and Turner, M. S. 1983, *Phys. Rev. D*, **28**, 679.
Bond, J. R. 1988, in *The Epoch of Galaxy Formation, Proc. NATO Advanced Research Workshop* (Durham), ed. C. F. Frenk *et al.* (Dordrecht: Kluwer).
Bond, J. R., and Efstathiou, G. 1984, *Ap. J. (Letters)*, **285**, L45.
———. 1987, *M.N.R.A.S.*, **226**, 655.
Bouchet, F. R., Bennett, D. P., and Stebbins, A. 1988, *Nature*, **335**, 410.
Brandenberger, R. H. 1988, in *The Epoch of Galaxy Formation, Proc. NATO Advanced Research Workshop* (Durham), ed. C. F. Frenk *et al.* (Dordrecht: Kluwer).
Cole, S., and Kaiser, N. 1988, *M.N.R.A.S.*, **233**, 637.
Coles, P. 1988, *M.N.R.A.S.*, **234**, 509.
Coles, P., and Barrow, J. D. 1987, *M.N.R.A.S.*, **228**, 407.
Cramer, H., and Leadbetter, M. R. 1965, *Ann. Math. Stat.*, **36**, 1656.
Dragovan, M. 1989, private communication.
Fixen, D. J., Cheng, E. S., and Wilkinson, D. J. 1983, *Phys. Rev. Letters*, **50**, 620.
Gorski, K., and Silk, J. 1989, *Berkeley* preprint.
Gott, J. R. 1982, *Nature*, **295**, 304.
———. 1985, *Ap. J.*, **288**, 422.
———. 1986, in *Inner Space/Outer Space, The Interface between Cosmology and Particle Physics*, ed. E. W. Kolb, M. S. Turner, D. Lindley, K. Olive, and D. Seckel (Chicago: University of Chicago Press), p. 362.
Gott, J. R., Melott, A. L., and Dickinson, M. 1986, *Ap. J.*, **306**, 341.
Gott, J. R., Miller, J., Thuan, T. X., Schneider, S. E., Weinberg, D. H., Gammie, C., Polk, K., Vogeley, M., Jeffrey, S., Bhavsar, S. P., Melott, A. L., Giovanelli, R., Haynes, M. P., Tully, R. B., and Hamilton, A. J. S. 1989, *Ap. J.*, **340**, 625.
Gott, J. R., and Statler, T. S. 1984, *Physics Letters*, **136B**, 157.
Grinstein, B., and Wise, M. 1987, *Ap. J.*, **320**, 448.
Hamilton, A. J. S., Gott, J. R., and Weinberg, D. H. 1986, *Ap. J.*, **309**, 1.
Ikeuchi, S. 1981, *Pub. Astr. Soc. Japan*, **33**, 211.
Kaiser, N., and Stebbins, A. 1984, *Nature*, **310**, 391.
Kofman, L. A., and Linde, A. D. 1987, *Nuc. Phys.*, **B282**, 555.
Leadbetter, M. R., and Cryer, J. D. 1965, *Bull. Amer. Math. Soc.*, **71**, 561.
Longuet-Higgins, M. S. 1957, *Phil. Trans. Roy. Soc. London A*, **249**, 321.
Lubin, P., Villela, T., Epstein, G., and Smoot, G. 1985, *Ap. J. (Letters)*, **298**, L1.
Melott, A. L., Cohen, A. P., Hamilton, A. J. S., Gott, J. R., and Weinberg, D. H. 1989, *Ap. J.*, **345**, 618.
Melott, A. L., Weinberg, D. H., and Gott, J. R. 1988, *Ap. J.*, **328**, 50.
Novikov, I. D. 1968, *Soviet Astr.*, **12**, 427.
Ostriker, J. P., and Cowie, L. L. 1981, *Ap. J. (Letters)*, **243**, L127.
Ostriker, J. P., Thompson, C., and Witten, E. 1986, *Phys. Lett.*, **B180**, 231.
Ostriker, J. P., and Vishniac, E. T. 1986, *Ap. J. (Letters)*, **306**, L51.
Park, C., and Gott, J. R. 1990, in preparation.
Peebles, P. J. E., 1982, *Ap. J.*, **259**, 442.
———. 1982, *Ap. J. (Letters)*, **263**, L1.
———. 1987, *Ap. J. (Letters)*, **277**, L1.
———. 1988, in *Large-Scale Structure and Motions in the Universe, Proc. Internat. Meeting* (Trieste), ed. M. Mezzetti, G. Giuricin, and F. Mardirossian, and M. Ramella (Dordrecht: Kluwer), p. 119.
Penzias, A. A., and Wilson, R. W. 1965, *Ap. J.*, **142**, 419.
Readhead, A. C. S., Lawrence, C. R., Myers, S. T., Sargent, W. L. W., Hardebeck, H. E., and Moffet, A. T. 1988, preprint, No. 23.
Ryden, B. S. 1988, *Ap. J. (Letters)*, **333**, L41.
Ryden, B. S., Melott, A. L., Craig, D. A., Gott, J. R., Weinberg, D. H., Scherrer, R. J., Bhavsar, S. P., and Miller, J. M. 1989, *Ap. J.*, **640**, 647.
Salopek, D. S., Bond, J. R., and Bardeen, J. M. 1988, preprint.
Sazhin, M. V. 1985, *M.N.R.A.S.*, **216**, 25p.
Scaramella, R., and Vittorio, N. 1988, *Ap. J. (Letters)*, **331**, L53.
Smoot, G., and Lubin, P. 1979, *Ap. J. (Letters)*, **234**, L83.

Starobinskii, A. 1982, *Phys. Lett.*, **117B**, 175.
Strukov, I. A., Skulachev, D. P., and Klypin, A. A. 1987, *IAU Symposium 130, Large-Scale Structures of the Universe*, ed. J. Audouze, M. Pelletan, and A. Szalay (Dordrecht: Kluwer), p. 27.
Sunyaev, R. A. 1978, in *IAU Symposium 79, The Large-Scale Structure of the Universe*, ed. M. S. Longair and J. Einasto (Dordrecht: Reidel), p. 393.
Sunyaev, R. A., and Zel'dovich, Ya. B. 1970, *Ap. Space Sci.*, **7**, 3.
Uson, J. M., and Wilkinson, D. T. 1984, *Ap. J. (Letters)*, **277**, L1.
Vishniac, E. T. 1987, *Ap. J.*, **322**, 597.
Vittorio, N., and Juszkiewicz, R. 1987, *Ap. J. (Letters)*, **314**, L29.
Wilkinson, D. T. 1988, *IAU Symposium 130, Large-Scale Structures of the Universe*, ed. J. Audouze, M. Pelletan, and A. Szalay (Dordrecht: Kluwer), p. 7.
Willmore, T. J. 1982, *Total Curvature in Riemanian Geometry* (New York: Ellis Horwood).
Wilson, M. L. 1983, *Ap. J.*, **273**, 2.

D. P. BENNETT and W. E. BIES: Physics Department and Department of Astrophysical Sciences, Princeton University, Princeton, NJ 08544

F. R. BOUCHET: Institut d'Astrophysique de Paris, 98 bis Blvd Arago, 75014 Paris

J. R. GOTT III and C. PARK: Department of Astrophysical Sciences, Princeton University, Princeton, NJ 08544

R. JUSZKIEWICZ: Institute for Advanced Study, Princeton, NJ 08540

A. STEBBINS: Canadian Institute for Theoretical Astrophysics, University of Toronto, McLennan labs, 60 St. George Street, Toronto, Ontario Canada M5S 1A1